Spin observables in small-angle elastic $\vec{p}\vec{d} \rightarrow \vec{p}d$ with an N-type polarized target at 800 MeV

G. Igo,[a] A. Masaike,[b]* B. Aas,[a]† D. Adams,[a]‡ E. Bleszynski,[a] M. Bleszynski,[a] M. Gazzaly,[c] S. J. Greene,[d] H. Hasai,[e] S. Ishimoto,[b] S. Isagawa,[b] K. Jones,[d] D. Lopiano,[a]§ J. B. McClelland,[d] F. Nishiyama,[e] Y. Ohashi,[a]§ A. Okihana,[f] G. Pauletta,[a]** F. Sperisen,[a]†† Tsu-Hsun Sun,[g] N. Tanaka,[d] G. S. Weston,[a]‡‡ and C. A. Whitten, Jr.[a]

[a]*Department of Physics, University of California at Los Angeles, Los Angeles, California 90024*

[b]*National Laboratory for High Energy Physics, KEK, Oho-machi, Tsukuba-gun, Ibarakiken, 305 Japan*

[c]*Department of Physics, University of Minnesota, Minneapolis, Minnesota 55455*

[d]*Los Alamos National Laboratory, Los Alamos, New Mexico 87545*

[e]*Hiroshima University, Hiroshima 730, Japan*

[f]*Kyoto University of Education, Fukakusa Fujinomori-cho, Fushimi-ku, Kyoto 606, Japan*

[g]*Institute of Atomic Energy, People's Republic of China, Academia Sinica, Peking, People's Republic of China*

(Received 6 July 1988)

The elastic scattering of 800 MeV polarized protons, with longitudinal, normal, and sideways orientations, from deuterons polarized normal to the scattering plane has been measured. The four-momentum transfer interval measured in this experiment is from 0.03 to 0.17 $(\mathrm{GeV}/c)^2$. Spin-correlation and spin-transfer observables have been extracted from the data. This experiment is one of a series designed to determine a number of observables in excess of the minimum number required to reconstruct the 12 subamplitudes of the proton-deuteron elastic scattering amplitude directly from spin observables. A comparison of the data with theoretical calculations employing three different phase-shift solutions for NN amplitudes reveals that sizable ambiguities exist in the values of NN amplitudes at small momentum transfers.

I. INTRODUCTION

The steady accumulation of n-p and p-p elastic scattering data in the intermediate energy range has constantly improved the accuracy of the phase-shift analyses of nucleon-nucleon (NN) scattering amplitudes.[1,2] Because of this situation, nucleon-nucleus scattering is generally considered as a source of information on processes specific to few- or many-nucleon systems. Indeed, important information on the latter phenomena can be extracted from measurements at sufficiently large momentum transfers where multiple scattering (as contrasted to single scattering) dominates. In particular, spin observables for momentum transfers squared $-t \gtrsim 0.3$ $(\mathrm{GeV}/c)^2$ in p-d elastic scattering constitute a rich source of information on those properties of nuclear forces (three-nucleon interactions, of-mass-shell effects) which cannot be derived from two-body scattering observables.[3]

The measurements presented in this paper have been made in the four-momentum transfer region where single scattering dominates. Therefore, as expected, the data presented here are mainly sensitive to the properties of the on-mass-shell nucleon-nucleon interaction. A comparison with the theoretical calculations discussed in Sec. IV reveals that the measurements *provide new information on the small momentum transfer NN amplitudes.* We find that in the range of momentum transfers squared covered, there are substantial differences between the predictions of the spin-dependent cross sections for p-d scattering coming from existing phase-shift analyses of NN data. Further, the present data, along with other observables measured in the small momentum transfer region, have definite value in the determination of the p-d scattering amplitudes at 800 MeV.

II. FORMALISM

Spins are expressed in two right-handed coordinate systems $(\hat{\mathbf{S}},\hat{\mathbf{N}},\hat{\mathbf{L}})$—one for the incident proton and target deuteron and another for the scattered proton. The polarization of the recoil deuteron was not measured. In each case, the longitudinal unit vector $\hat{\mathbf{L}}$ is parallel to the proton laboratory momentum ($\vec{k}_i$ for the incident and $\vec{k}_f$ for the scattered proton). The normal vector unit vector $\hat{\mathbf{N}}$ is perpendicular to the scattering plane along the direction $\vec{k}_i \times \vec{k}_f$. The sideways direction is defined by $\hat{\mathbf{S}} = \hat{\mathbf{N}} \times \hat{\mathbf{L}}$. We note that $\hat{\mathbf{S}}$ and $\hat{\mathbf{L}}$ change sign under a parity transformation, while $\hat{\mathbf{N}}$ is unaffected. A complete set of spin-$\frac{1}{2}$ operators for the proton are given by σ_a $(a = 0,S,N,L)$. Here $\sigma_0 = 1$ is the identity operator and $\sigma_i = \vec{\sigma}\cdot\hat{\mathbf{i}}$ $(i = S,N,L)$, where $\vec{\sigma}$ is the spin-$\frac{1}{2}$ Pauli vector operator. The density matrix describing a mixture of spin-$\frac{1}{2}$ particles may be expressed in terms of the polarization vector (p_S,p_N,p_L) as follows:

$$\rho^{(p)} = \tfrac{1}{2}(1 + p_S\sigma_S + p_N\sigma_N + p_L\sigma_L) .$$

The polarization components are defined by the relations

$$p_i = \langle \sigma_i \rangle = \frac{\mathrm{Tr}(\rho\sigma_i)}{\mathrm{Tr}(\rho)} .$$

Three spin-1 operators are sufficient to describe the state of our deuteron target, because the polarizing field was cylindrically symmetric about the $\hat{\mathbf{N}}$ direction.

These operators are the identity operator $\hat{1}$, the $\hat{\mathbf{N}}$ component of the spin-1 vector operator, $J_N=\vec{J}\cdot\hat{\mathbf{N}}$, and the tensor operator $J_{NN}=3J_N^2-2$. The density matrix describing the target can be expressed in terms of the vector polarization $P_N=\langle J_N\rangle$ and the tensor polarization $P_T=\langle J_{LL}\rangle$:

$$\rho^{(d)}=\tfrac{1}{3}(1+\tfrac{3}{2}PJ_N+\tfrac{1}{2}P_TJ_{NN}) .$$

The density matrix describing the initial proton-deuteron system is just the product of the proton and deuteron density matrices. The observables are defined in terms of the scattering matrix F:

$$C(a,\alpha,b,\beta)=\frac{\mathrm{Tr}(F\sigma_aJ_\alpha F^\dagger\sigma_bJ_\beta)}{\mathrm{Tr}(FF^\dagger)} .$$

The density matrix describing the final particles ρ' is obtained from the scattering matrix and the initial state density matrix as follows:

$$\rho'=F\rho F^\dagger .$$

The relative yield or the cross section is given by

$$Y=\mathrm{Tr}(\rho') ,$$

and the components of the polarization of the scattered proton are

$$p_i'=\frac{\mathrm{Tr}(\rho'\sigma_i)}{\mathrm{Tr}(\rho')} .$$

By assuming parity conservation one gets the following expressions for the yield and for the components of polarization of the scattered particles in terms of their initial state polarizations:

$$\begin{aligned}Y=Y_0[1&+p_NC(N,0,0,0)+\tfrac{3}{2}PC(0,N,0,0)\\&+\tfrac{1}{2}P_TC(0,NN,0,0)+\tfrac{3}{2}p_NPC(N,N,0,0)\\&+\tfrac{1}{2}p_NP_TC(N,NN,0,0)] ,\end{aligned}\tag{1}$$

$$\begin{aligned}p_S'=\frac{Y_0}{Y}\{&p_S[C(S,0,S,0)+\tfrac{3}{2}PC(S,N,S,0)\\&+\tfrac{1}{2}P_TC(S,NN,S,0)]\\&+p_L[C(L,0,S,0)+\tfrac{3}{2}PC(L,N,S,0)\\&+\tfrac{1}{2}P_TC(L,NN,S,0)]\} ,\end{aligned}\tag{2}$$

$$\begin{aligned}p_N'=\frac{Y_0}{Y}\{&C(0,0,N,0)+\tfrac{3}{2}PC(0,N,N,0)\\&+\tfrac{1}{2}P_TC(0,NN,N,0)\\&+p_N[C(N,0,N,0)+\tfrac{3}{2}PC(N,N,N,0)\\&+\tfrac{1}{2}P_TC(N,NN,N,0)]\} ,\end{aligned}\tag{3}$$

$$\begin{aligned}p_L'=\frac{Y_0}{Y}\{&p_S[C(S,0,L,0)+\tfrac{3}{2}PC(S,N,L,0)\\&+\tfrac{1}{2}P_TC(S,NN,L,0)]\\&+p_L[C(L,0,L,0)+\tfrac{3}{2}PC(L,N,L,0)\\&+\tfrac{1}{2}P_TC(L,NN,L,0)]\} .\end{aligned}\tag{4}$$

Here Y_0 denotes the yield that would be obtained with unpolarized beam and target. These equations are the basis for extracting the observables from our data as described in Sec. IV.

III. EXPERIMENT

The experiment was performed at the high-resolution spectrometer (HRS) facility at Los Alamos Meson Physics Facility (LAMPF) utilizing the focal plane polarimeter (FPP) at the HRS. The measurements were made in the angular range (forward angles) where the recoil deuteron does not have sufficient kinetic energy, because of the finite thickness of the target and of the cryostat walls, to be detected, i.e., $-t<0.2$ (GeV/c).[2] Measurements at larger four-momentum transfer can be accomplished without benefit of a high-resolution magnetic analysis system. Since data-taking time at the HRS facility is always well booked, only the small t region was investigated in this experiment.

Figure 1 illustrates a schematic reproduction of the target region at HRS adapted for these measurements. The large diameter scattering chamber was removed and a polarizing and holding dipole magnet was put in its place. The purpose of the dipole magnet was to generate a 2.5-T field, normal to scattering plane, for polarizing the target or alternatively a 1.0-T holding field. The target consisted of a teflon flask, 48 mm along the beam axis and 20 mm by 25 mm (height) in cross section, filled with fully deuterated propanediol, with a packing fraction of 0.7. A ^{3}He-^{4}He dilution refrigerator[4] was used to cool the target to a temperature in the 50-mK range. At this temperature, the nuclear spin relaxation time is quite long ($\sim$100 h in a 1-T magnetic field). The data were obtained in the frozen spin mode with a field of 1 T.

The primary method used for determining the target polarization was to measure the deuteron vector asymmetry in proton-deuteron scattering. The deuteron vector analyzing power $C(0,N,0,0)$ had previously been measured utilizing a polarized deuteron beam.[5,6] It is largest at 0.1 (GeV/c)^2 in the range measured in the ex-

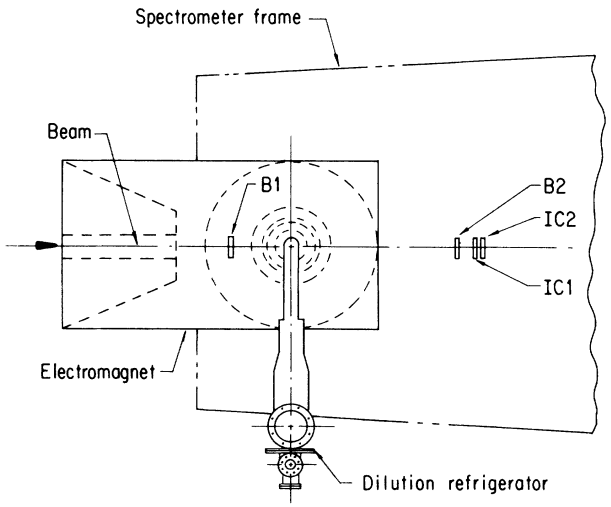

FIG. 1. A schematic diagram of the polarized target facility used in this experiment.

periment of Refs. 5 and 6. By measuring the left-right asymmetry at $-t=0.1$ (GeV/c)^2, the target vector polarization P could be determined from Eq. (1). The tensor component P_T is related to P, assuming a Boltzmann distribution of the target deuteron spins, while the tensor analyzing power $C(0,NN,0,0)$ is known from previous measurements.[6]

In order to reduce depolarization effects in the target due to heating from the protons passing through it, the beam (1 mm wide $\times$10 mm high) was swept horizontally with a 10-mm amplitude at the target at a frequency of 1 Hz. Even then the volume of the target struck by the beam was significantly less than the overall volume of the target. A deuteron magnetic resonance (DMR) pickup loop wrapped around the target was also used to monitor the beam polarization. The loop preferentially samples the polarization of the target nearest the surface. Thus the depolarization of the target caused by beam heating is not accurately proportional to the DMR signal since the beam was restricted to a one-square-centimeter cross-sectional area in the central part of the target. The DMR signals were calibrated by fitting them, extracting the asymmetry of the transition intensities between the magnetic substates.[7]

The target polarization was checked after the bombardment of the target for 10–12 h. The primary method was described above, involving an asymmetry measurement with HRS. Following this, the field was increased to 2.5 T and the DMR signal was measured. The latter was a particularly useful thing to do just after the target had been repolarized, when the two methods should agree. We found good agreement, within the statistical uncertainty of the scattering results, when the target had been polarized starting from zero. After repolarizing from a nonzero polarization, however, the DMR values were considerably higher than those from the scattering asymmetry, indicating a nonhomogeneous distribution of the polarization over the target volume. The asymmetry measurements clearly displayed a linear decrease in the target polarization, of about a percent per two hours at a beam level of 5×10^6 sec^{-1}.

The beam polarization components in the normal ($\hat{\mathbf{N}}$) and sideways ($\hat{\mathbf{S}}$) directions were determined by a conventional double arm polarimeter which measures the left-right asymmetry in p-p elastic scattering using a CH_2 target. This polarimeter was upstream of the HRS target region displayed in Fig. 1. The beam polarization is expressed in terms of the measured quantities: the magnitude of the beam polarization, p_B, the N component p_N, and the S component, p_S. The magnitude p_B was determined from quench measurements[8] taken cyclically with data runs utilizing opposite beam polarization. Quench measurements require knowledge of the beam flux. The beam intensity was monitored by the current generated in two ion chambers (IC1 and IC2 in Fig. 1). The beam intensity was typically 5×10^6 sec^{-1}. To enhance the ion chamber response, the chambers were filled with heavy noble gases; one with Xe and the other with Kr. A comparison of the currents from the two chambers provided a check that the chamber with the heavier gas filling (Xe) was not saturating.

The statistical uncertainties in the beam polarization measurements are quite small, but the quench measurements are subject to other errors which are difficult to evaluate precisely. Most important is the normalization, which can be in error if there are many empty cycles or if the beam is changing on a time scale of a few minutes. An uncertainty of 0.02 was attributed to the quench measurements for each series of runs.

Just as in the case of the target polarization, where redundant information was obtained from measuring the DMR signal, it was desirable to incorporate redundancy into the measurement of the beam polarization. This was accomplished by utilizing measurements with polarimeters on two other beam lines and from their respective quenches. These beam lines share the polarized negative ion beam with the HRS facility. This procedure was particularly advantageous when an L-type beam was used. In this case the small components ($\hat{\mathbf{N}}$ and $\hat{\mathbf{S}}$) arising from the misalignment of the beam's polarization direction can be measured by the HRS beam polarimeter, but the quench measurement provides the only measurement available at the HRS facility of the large component ($\hat{\mathbf{L}}$). However, in one of the two remaining beam lines, the beam is precessed through approximately $\pi/2$ at the location of that beam polarimeter. The large component, now in the S direction, can be measured by a beam polarimeter in that area. However, uncertainty arises, since the HRS beam is produced by utilizing a stripper foil or screen to strip a portion of the negative hydrogen ion beam before this beam enters into the other two lines. If a narrow stripper foil is used, the HRS beam does not necessarily come from the same part of the beam phase space as the portion sent to other areas. Whenever intensity requirements allowed, we used a screen covering the entire area of the beam as a stripper in order to sample the entire phase space of the beam which helps to reduce this ambiguity.

Care was taken to ensure that the region in which the beam intercepted the target was within the acceptance of the spectrometer. In order to accomplish this, x-ray photographs were taken of the position of the target within the cryostat, and then the cooled cryostat was surveyed into place. The position of the beam was aligned precisely (±1 mm) on the target by exposing film (Type 57 High Speed 4 in. $\times$5 in. LAND Film, Polaroid Corporation, Cambridge, MA 02139) secured to the cryostat, to the beam, and adjusting the direction and location of the beam until the image was located properly. During the data taking the position and shape of the beam were continuously monitore d by the beam profile monitors ($B1$ and $B2$ in Fig. 1).

IV. DATA ANALYSIS AND EXPERIMENTAL RESULTS

The experimental observables were reduced from 533 tapes (1600 bpi) taken with a polarized, fully deuterated propanediol (D-propanediol) target, and 81 tapes with unpolarized propanediol material with hydrogen atoms replacing the deuterium atoms (H-propanediol). In the latter case, required for background subtraction (see below), only an $\hat{\mathbf{N}}$-type beam was employed. In this case,

the cryostat was cooled to the temperature of liquid nitrogen only (no ^{3}He-^{4}He liquid in the cryostat). The 1-T holding field, utilized during data taking with the polarized D-propanediol target, was kept on. The FPP was not required and therefore not used for these background runs.

Figure 2 shows a typical energy spectrum from the emas (note the baseline suppression). In addition to the elastic deuteron peak and a broad distribution from deuteron breakup, elastic scattering contributions from the ^{3}He and ^{4}He in the cryostat and a smooth underlying background, originating from inelastic scattering on the heavier elements of deuterated propanediol (C and O) and the target walls, are indicated. This background shows little or no structure for two reasons. One, in the analysis, the kinematic energy shifts with angle for a given missing mass are corrected for as if all scattering occurs from deuterium into the 1.6° angular acceptance, and therefore all possible spectral lines from heavy elements are washed out. Even at small angles, the proton momentum corresponding to p-d elastic scattering is about the same as that corresponding to p-heavy element inelastic scattering to states (structures) with quite high excitation energies and therefore large widths. Therefore this relatively structureless background facilitates the background subtraction procedure.

The spectrum in Fig. 2 was taken at 12.5°. At this angle, the ^{3}He peak is well resolved from the deuteron peak. The ^{3}He level in the cryostat was not controlled and was not expected to be constant with time. The consequence was that the magnitude of the ^{3}He peak in the energy spectra varied in an unpredictable way. This caused an increase in the error for observables measured at 7°, where the ^{3}He peak was not well resolved from the deuteron peak.

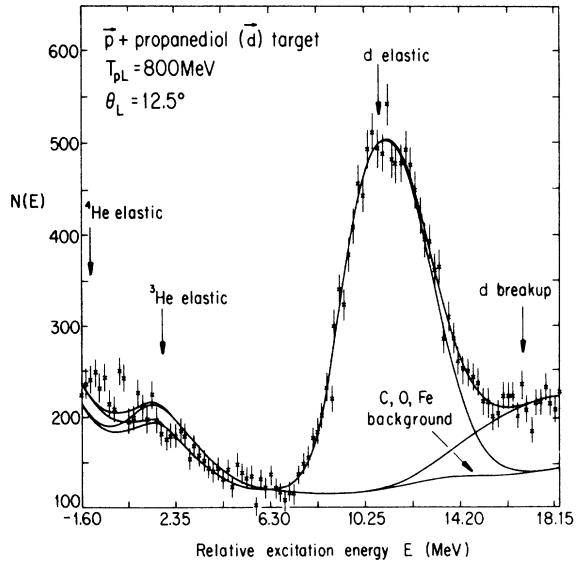

FIG. 2. Spectrum obtained at $\theta_2 = 12.5°$. The location of the elastic peaks for ^{4}He, ^{3}He, and ^{2}H are indicated. The background obtained utilizing H-propanediol is shown and labeled "C, O, Fe Background" in the figure. Also shown is the contribution from deuteron breakup. The solid curves illustrate the elastic peak and the background components as well as the composite spectrum.

The energy spectra were fit with a modified version of the computer code ALLFIT.[9] The overall features of the prominant peak due to elastic proton-deuteron scattering, appearing at each angle in the spectra, were parametrized first. Then the parameters of the deuteron breakup distribution were chosen empirically in a fashion to fit the spectra reasonably well. The deuteron breakup distribution is constant more than 4 MeV away from the center of the deuteron peak, and decreases linearly to zero at the center beginning 3 MeV away. This distribution is folded with the shape of the elastic deuteron peak distribution. Since the breakup extends under the elastic peak, the area of the elastic peak will be somewhat dependent on the choice of the parameters for the breakup distribution. Asymmetries, obtained by combining normal and reverse beam polarization measurements, turn out to be insensitive to these parameters.

The ^{3}He and ^{4}He peaks were slightly broadened due to the kinematic effect mentioned above. The "heavy element" background was determined from the background runs, i.e., by utilizing the H-propanediol data.

As discussed above, the vector polarization of the target was determined by frequent left-right asymmetry measurements, with the HRS placed at an effective scattering angle of $\pm 12.5°$. The vector analyzing power for deuterium at this angle and energy was taken as the average of the measurements of Refs. 6 and 10, which were themselves consistent with one another,

$$A_y^T = 0.357(19) . \tag{5}$$

As a consequence of the errors assigned in Ref. 6, there is a 5% uncertainty introduced in the normalization of the data presented in this paper. The statistical (relative) uncertainties from our asymmetry measurements were typically 5–10 %. They were larger when the target was polarized with spin down than with spin up. This was because higher target polarization was obtained for spin up than for spin down.

The target vector polarization was typically 20–30 % for spin up and 10–20 % for spin down. With deuteron vector polarization $\lesssim 30\%$, the magnitude of the deuteron target tensor polarization will be $\lesssim 7\%$. Because of this very low polarization, we were not able to extract useful measurements of tensor quantities from this experiment.

During the early part of the experiment, when we obtained our data with $\hat{\mathbf{N}}$-type beam and about 50% of our data with $\hat{\mathbf{S}}$-type beam, the HRS was positioned to measure left scattering only (except for the asymmetry measurements discussed above), and the target spin was polarized sequentially up and down. After it was verified that substantially larger target polarization occurred for spin up, left-right measurements were performed keeping the target polarized with spin up. Because of rotational symmetry, the two methods are equivalent.

In order to determine the polarization components of the elastically scattered protons, a gate was set within the deuteron peak in the energy spectrum, with a width

slightly larger than its half-width. The centroid of the gate did not coincide with the peak of the deuteron spectrum, instead it was shifted slightly in order to exclude some deuteron breakup events. Utilizing the measurements made with the FPP, the components of polarization of the protons within this gate were determined, i.e., the average value for peak and background within the gate. In order to determine the proper background subtraction, we measured yields from an (unpolarized) H-propanediol target, and from a polarized and from an unpolarized D-propanediol target, at all angular settings.

The beam-target spin correlation parameters $C(a,\alpha,0,0)$ have been obtained by linear least-squares calculation based on yields given by Eq. (1). In principle, all five polarization observables in Eq. (1) are determined by the combinations of beam and target polarizations of our experiment. However, the tensor observable $C(N,NN,0,0)$ could not be extracted reliably from our data. Due to its extreme sensitivity to the beam intensity normalization from run to run, the values obtained for this observable had a distribution much broader than what would correspond to the counting statistical error of 0.5. The correlation parameter $C(N,N,0,0)$ was extracted from asymmetry ratios

$$\frac{Y^{(n)}-Y^{(r)}}{Y^{(n)}+Y^{(r)}}=\frac{p_N[C(N,0,0,0)+\frac{3}{2}PC(N,N,0,0)+\frac{1}{2}P_TC(N,NN,0,0)]}{\frac{3}{2}PC(0,N,0,0)+\frac{1}{2}P_TC(0,NN,0,0)} . \tag{6}$$

The superscripts n and r refer to normal and reversed beam polarization. For $C(0,N,0,0)$ and $C(0,NN,0,0)$ interpolated values from Refs. 5 and 6 were used. Due to the frequent reversal of the beam polarization, the ratios (6) are not sensitive to the beam intensity normalization from run to run.

The second class of observables, $C(a,\alpha,b,0)$ with $b\neq 0$, are determined by Eqs. (2), (3), and (4). For the actual data reduction, however, these equations had to be modified in order to account for the two following problems.

(i) The measured FPP polarizations are mixtures from protons from both p-d elastic and background scattering.

(ii) Proton spins are precessed in the holding field of the polarized target and in the two HRS dipoles.

In dealing with the first problem, it can be shown that Eqs. (2), (3), and (4) need to be understood as follows, in order to give correctly the measured polarization mixtures p_i'.

(a) Y is to be taken as the total yield of protons (background included) accepted for FPP scattering by the gates set in the energy spectrum.

(b) Y_0 is the yield of accepted protons originating from p-d elastic scattering (background subtracted), that would be obtained with both beam and target *unpolarized*. Y_0 has been determined from the measured polarized yield by Eq. (1). The beam-target correlation of observables appearing in Eq. (1) thus have to be assumed known parameters in determining the FPP observables. The unknown tensor observable $C(N,NN,0,0)$ was shown to have a negligible effect on the resulting values for the FPP observables, when allowed to vary within its boundaries of ± 2.

(c) All observables $C(a,\alpha,b,0)$ with $\alpha=0$ have to be substituted by corresponding expressions

$$C^{pd}+\frac{(Y_0^{\rm bu}C^{\rm bu}+Y_0^{\rm bg}C^{\rm bg})}{Y_0^{pd}} ,$$

where the superscripts pd, bu, and bg refer to p-d elastic scattering, p-d breakup, and other background scattering, respectively; Y_0 denotes the corresponding unpolarized yield. This means that these observables, which do not refer to the initial deuteron polarization ($\alpha=0$), cannot be extracted for p-d elastic scattering from this experiment. However, these observables (Wolfenstein parameters and induced polarization) have been measured previously[11] by using an unpolarized liquid deuterium target.

(d) The observables of interest, namely $C(a,\alpha,b,0)$ with $\alpha\neq 0$, have to be read as

$$C^{pd}+\frac{Y_0^{\rm bu}}{Y_0^{pd}}C^{\rm bu} .$$

Thus, even in this case, we do not get pure p-d elastic scattering observables, because of the inseparable admixture from the breakup process. However, this contribution may be considered negligibly small in relation to the statistical uncertainties of the present results, as the ratio $Y_0^{\rm bu}/Y_0^{pd}$ was normally less than 5%. The results given in this paper are actually for observable combinations as given above.

The second modification of Eqs. (2), (3), and (4) concerns the precession of the incident and outgoing proton spins. The 1-T holding field of the polarized target caused the polarization components in the scattering plane to rotate by 8.5° for the incident beam, and between 8.53° and 8.61° for the scattered beam. These precession angles were determined from the corresponding deflection (5.08° for the incident beam), which in turn were found in a measurement of the position of the first minimum in the differential cross section for p-^{208}Pb elastic scattering, with and without the holding field, using a thin ^{208}Pb foil as a target.

Finally, mixing of the $\hat{\mathbf{N}}$ and $\hat{\mathbf{L}}$ components of the scattered polarization occurs in the HRS dipoles, which deflect the protons by approximately 150° in a vertical plane, resulting in a precession angle around 490°, slightly varying with the scattering angle.

In order to extract the wanted observables, each of the two transverse FPP polarization components were expressed as a linear combination of all observables that appear in Eqs. (2), (3), and (4). A computer program was written to perform a linear least-squares calculation.

The electronics associated with the multiple wire drift chambers (MWDC's) of the HRS FPP were not completely stable during part of the experiment, requiring frequent recalibrations, sometimes as often as every 12 h of running time. This could be done during the analysis after the experiment, and did not constitute a real problem. A more serious problem was associated with position-dependent inefficiencies. These were also drifting, causing time-dependent instrumental asymmetries. Fortunately this source of false asymmetries does not affect most of the observables; those observables where this effect cancels by averaging over polarization measurements with normal and reverse beam polarization. All terms involving C variables which are odd in the beam polarization are in this category [see Eqs. (5)–(7)]. Only $C(0,N,N,0)$ is strongly affected. However, three independent measurements of this observable are available in our data sample, one for each beam polarization. The spread in numerical values from the three different measurements of $C(0,N,N,0)$ determined the contribution to the error due to fluctuations in the instrumental asymmetry discussed above. Summarizing this discussion, it was found that due to fluctuations in the instrumental asymmetries, the uncertainty in $C(0,N,N,0)$ is increased by a factor of 2 at all angles except 16.5°, where the increase was a factor of 3. The contribution to the error for $C(N,N,N,0)$, the only other C variable which is affected, is quite small, 10–20 %.

V. SUMMARY OF RESULTS OF THIS EXPERIMENT AND OF OTHER MEASUREMENTS COVERING THE SAME FOUR-MOMENTUM TRANSFER REGION

Previously unmeasured second- and third-order spin observables have been determined at small four-momentum transfers, $0.02 < -t < 0.17$ $(\mathrm{GeV}/c)^2$ (Ref. 12) at 800 MeV. The second-order observables include spin-correlation observable $C(N,N,0,0)$, one spin-transfer observable $C(0,N,N,0)$, and five third-order spin observables. The experimental data obtained are listed in Tables I–VII and are plotted in Figs. 3–9. These data have been obtained with an $\hat{\mathbf{N}}$-type polarized deuteron target. The curves presented in these figures were obtained by using the single collision approximation of Ref. 13. In the range of momentum transfers covered by our experiment the double scattering contribution is typically less than 10%. In Figs. 3–9, results of calculations are shown, utilizing three different sets of NN amplitudes. The solid curves and the short-dashed curves were obtained by using phase solutions SM86 and SP82 of Arndt *et al.*,[1] respectively. The long-dashed curves correspond to the phase-shift analysis of Bystricky *et al.*[2] We note that, while some of the observables are rather insensitive to the differences in the phase-shift solutions, several observables measured in our experiment exhibit considerable sensitivity to these differences. In particular the observable $C(N,N,0,0)$ shown in Fig. 3 favors solution SM86 (Ref. 1) and the same may be said of the observable $C(0,N,N,0)$ although with considerably less conviction. The same three calculations for the observable $C(N,N,N,0)$, shown in Fig. 5 are almost indistinguishable. The theoretical predictions for the observable $C(S,N,S,0)$, shown in Fig. 6 agree, in magnitude with the data only at the smallest momentum transfer. The observables, $C(S,N,L,0)$ and $C(L,N,S,0)$, shown in Figs. 7 and 8 differ systematically from the predictions with the phase-shift solution SP82 (Ref. 1) approximating the data most closely. As expected these two observables are approximately of the same magnitude and of opposite sign, in agreement with approximate relations following from time reversal and parity conservation symmetries. The measured values of the observable $C(L,N,L,0)$, shown in Fig. 9, poorly define the behavior of this observable, so no meaningful comparison can be made with the three calculations.

The significant differences between the predictions obtained using the three phase-shift solutions can be attributed to lack of small angle NN (p-n, in particular)

TABLE I. The second-order observable $C(N,N,0,0)$ as a function of the momentum transfer, $-t$, in elastic proton-deuteron scattering at 800 MeV. The evaluation of the error $\delta C(N,N,0,0)$ is discussed in the text.

$-t$ $(\mathrm{GeV}/c)^2$	$C(N,N,0,0)$	$\delta C(N,N,0,0)$
0.032	0.020	0.091
0.077	0.098	0.043
0.099	0.139	0.009
0.123	0.129	0.039
0.170	0.210	0.029

TABLE II. The second-order observable $C(0,N,N,0)$ as a function of the momentum transfer, $-t$, in elastic proton-deuteron scattering at 800 MeV. The evaluation of the error $\delta C(0,N,N,0)$ is discussed in the text.

$-t$ $(\mathrm{GeV}/c)^2$	$C(0,N,N,0)$	$\delta C(0,N,N,0)$
0.032	0.080	0.103
0.077	0.020	0.085
0.123	0.018	0.092
0.170	0.266	0.169

TABLE III. The second-order observable $C(N,N,N,0)$ as a function of the momentum transfer $-t$, in elastic proton-deuteron scattering at 800 MeV. The evaluation of the error $\delta C(N,N,N,0)$ is discussed in the text.

$-t$ $(\mathrm{GeV}/c)^2$	$C(N,N,N,0)$	$\delta C(N,N,N,0)$
0.032	0.333	0.089
0.077	0.357	0.102
0.123	0.135	0.125
0.170	0.557	0.213

TABLE IV. The second-order observable $C(S,N,S,0)$ as a function of the momentum transfer, $-t$, in elastic proton-deuteron scattering at 800 MeV. The evaluation of the error $\delta C(S,N,S,0)$ is discussed in the text.

$-t$ (GeV/c)^2	$C(S,N,S,0)$	$\delta C(S,N,S,0)$
0.032	0.200	0.051
0.077	0.426	0.050
0.123	0.319	0.061
0.170	0.469	0.098

TABLE VI. The second-order observable $C(L,N,S,0)$ as a function of the momentum transfer $-t$, in elastic proton-deuteron scattering at 800 MeV. The evaluation of the error $\delta C(L,N,S,0)$ is discussed in the text.

$-t$ (GeV/c)^2	$C(L,N,S,0)$	$\delta C(L,N,S,0)$
0.032	−0.61	0.055
0.077	−0.048	0.045
0.123	−0.006	0.060
0.170	−0.066	0.122

scattering data. From the inspection of Figs. 3–9, we conclude that the curves based on the SP82 solution are closest to the experimental points. In the case of some observables, however, none of the three calculations could be excluded on the basis of the data because of the sizable experimental uncertainties.

It is also interesting to compare the three sample calculations appearing in Figs. 3–9 with the data on other spin observables. Eight-hundred-MeV data have been obtained in the same four-momentum transfer domain utilizing an L-type polarized target.[12] In addition the Wolfenstein observables[14] $C(N,0,N,0)$, $C(S,0,S,0)$, $C(L,0,L,0)$, $C(S,0,L,0)$, and $C(L,0,S,0)$, and the unpolarized differential cross sections[15] have been measured at 800 MeV also covering a larger range of momentum transfers. The latter is shown in Fig. 11 where a comparison is made with the same three calculations discussed above. Inclusion of the double scattering part of the p-d collision amplitude, utilizing once again the SP82 solution, reproduces the data quantitatively.

Other 800-MeV measurements in this momentum transfer range include the asymmetry observables.[11,12,15–18] These are the proton asymmetry $C(N,0,0,0)$ (Fig. 10), the deuteron vector asymmetry, $C(0,N,0,0)$, and the deuteron tensor asymmetries, $C(0,NN,0,0)$ and $C(0,SS,0,0)$ (Figs. 12–14). The dotted curves displayed in Figs. 11–14 represent calculations based on the SP82 solution in which the double scattering on two target nucleons is included. Our calculations indicate that these observables, in contrast to those shown in Figs. 2–10, are quite sensitive to the double scattering term, even at these small momentum transfers. This can be seen particularly clearly in the tensor observables $C(0,NN,0,0)$ and $C(0,SS,0,0)$. In the case of $C(0,NN,0,0)$ there is still a systematic deviation between the data and the theoretical calculations. In concluding this section we reemphasize that in the case of these asymmetry variables the double scattering amplitudes are quite crucial even at very small momentum transfers, and their contributions are quite essential to bring the theoretical predictions close to the experimental points.

VI. SUMMARY OF PROTON-DEUTERON ELASTIC SCATTERING MEASUREMENTS WHICH PROVIDE DATA IN THE MOMENTUM TRANSFER RANGE $|t| \leq 0.7$ (GeV/c)^2

Two important objectives motivated the series of experiments the results of which were summarized in the last section. The first objective was to provide significant data which bear on the question of the behavior of the nuclear forces in the intermediate energy range, such as three-nucleon interactions.

The second objective, not completely uncoupled from the first, that we hope to accomplish at the completion of the measurements, is the experimental determination of the 12 complex components of the proton-deuteron elastic scattering amplitude (within an overall phase factor). Then it will be possible to reconstruct the proton-deuteron elastic scattering amplitude (up to an arbitrary overall phase factor) at 800 MeV for $|t| \leq 0.7$ (GeV/c)^2 with reasonable accuracy directly in terms of measured experimental observables. The overdetermination of the 12 complex components of the amplitude is crucial; this

TABLE V. The second-order observable $C(S,N,L,0)$ as a function of the momentum transfer, $-t$, in elastic proton-deuteron scattering at 800 MeV. The evaluation of the error $\delta C(S,N,L,0)$ is discussed in the text.

$-t$ (GeV/c)^2	$C(S,N,L,0)$	$\delta C(S,N,L,0)$
0.032	0.121	0.067
0.077	0.036	0.060
0.123	0.054	0.074
0.170	0.005	0.115

TABLE VII. The second-order observable $C(L,N,L,0)$ as a function of the momentum transfer, $-t$, in elastic proton-deuteron scattering at 800 MeV. The evaluation of the error $\delta C(L,N,L,0)$ is discussed in the text.

$-t$ (GeV/c)^2	$C(L,N,L,0)$	$\delta C(L,N,L,0)$
0.032	0.127	0.074
0.077	0.355	0.060
0.123	0.410	0.073
0.170	0.061	0.144

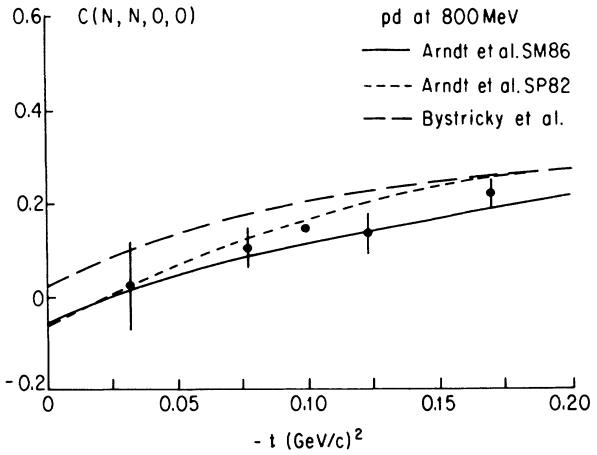

FIG. 3. Second-order (spin-correlation) observable $C(N,N,0,0)$ measured at the HRS using an $\hat{\mathbf{N}}$-type polarized deuteron target. The point at $|t|=0.1$ (GeV/c)^2 has a relatively small statistical error because it was measured in conjunction with $C(0,N,0,0)$ ($\theta_{\text{lab}}=12.5°$). The latter observable appears in the expression for the yield as a product with the deuteron target's vector polarization P_T^V. This quantity was measured frequently to determine the magnitude of P_T^V, i.e., before repolarizing the target, which normally occurred at the end of data accumulation at each angle setting. The solid curve and long-dashed curves represent calculations based on SM86 and SP86 NN phase-shift solutions of Ref. 1. The short-dashed curve corresponds to the NN phase shifts of Ref. 2.

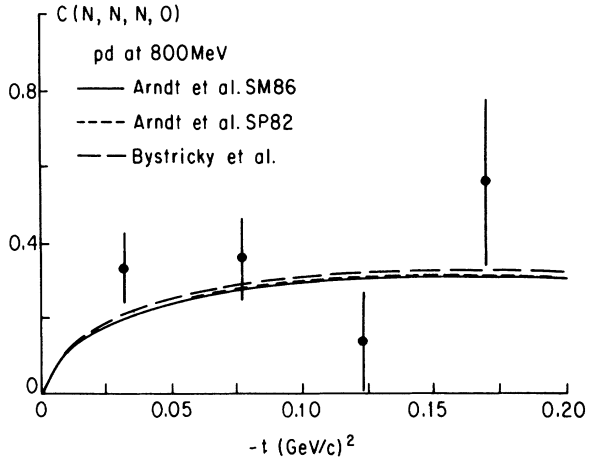

FIG. 5. The third-order spin observable, $C(N,N,N,0)$. See the caption of Fig. 3 for an explanation of the curves shown in this figure.

will result from a redundant set of observables to be provided in the data set. In the remaining part of this paper, we summarize other measurements in progress to accomplish this objective.

In the previous sections we have discussed comparisons of the data measured in the present experiment (Figs. 3–9) as well as the other existing small momentum transfer data (Figs. 10–14) with calculations using three sets of phase-shift solutions for NN amplitudes. We have discussed there how well or how poorly these observables are reproduced by the calculations based on different phase-shift solutions. The reader is reminded that a considerable amount of larger four-momentum transfer data [$0.2<|t|<0.7$ (GeV/c)^2] exist which are not presented in this paper. The data at larger values of $-t$ cover the region where double scattering predominates. Altogether the experiments discussed in Sec. V account for 26 observables in the momentum transfer region [$-t<0.2$

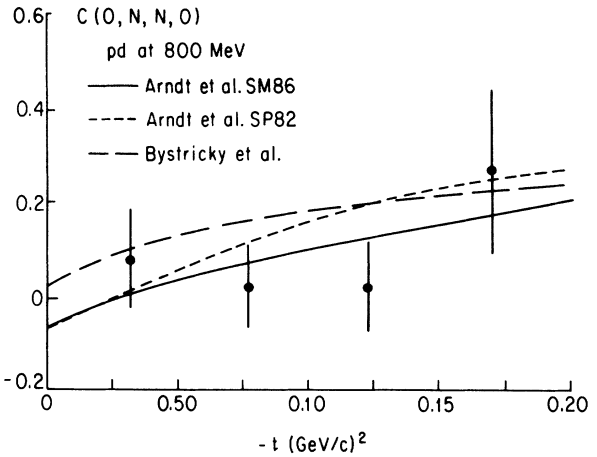

FIG. 4. The second-order (spin-transfer) observable, $C(0,N,N,0)$, measured with the $\hat{\mathbf{N}}$-type polarized target. See the caption of Fig. 3 for an explanation of the curves appearing in this figure.

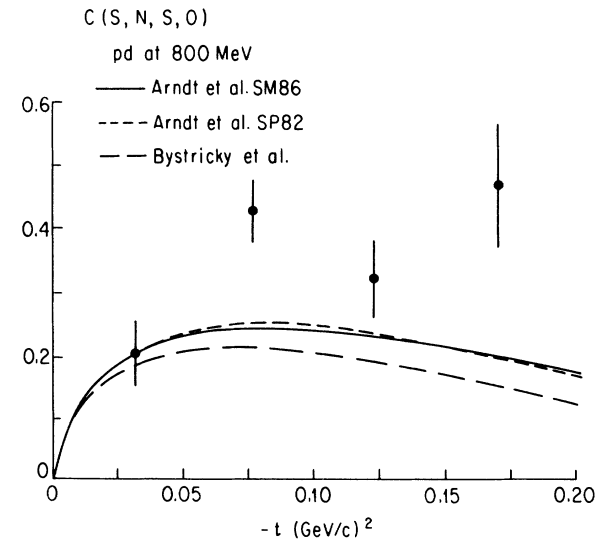

FIG. 6. The third-order spin observable, $C(S,N,S,0)$. See the caption of Fig. 3 for an explanation of the curves shown in this figure.

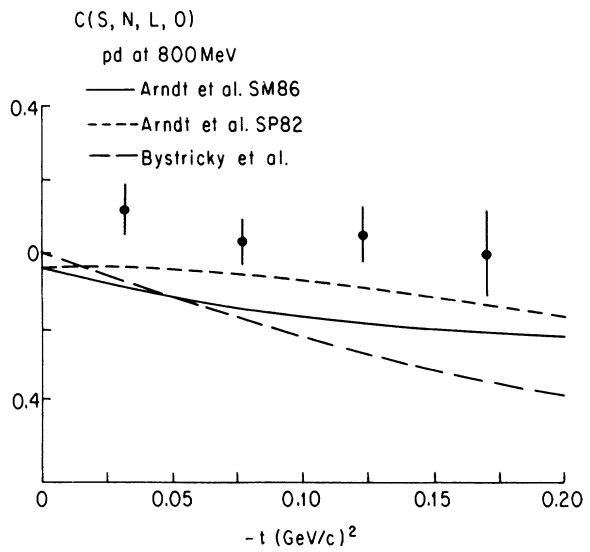

FIG. 7. The third-order spin observable, $C(S,N,L,0)$. See the caption of Fig. 3 for an explanation of the curves shown in this figure.

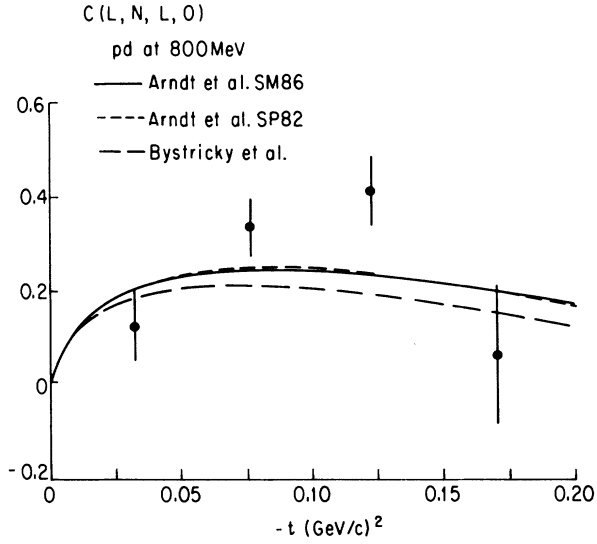

FIG. 9. The third-order spin observable, $C(L,N,L,0)$. See the caption of Fig. 3 for an explanation of the curves shown in this figure.

$(\mathrm{GeV}/c)^2$]. They have been shown to constitute a complete set (at least in the continuous sense) by using the method presented recently in Ref. 19. At least 23 observables are required to remove continuous ambiguities in the equations relating the amplitudes to the observables,[19] and a suitable number of other observables is needed to remove discrete ambiguities. In principle the latter task will require measurements over a restricted range of momentum transfers. The problem of choosing the most economical sets of observables needed to determine the collision matrix describing p-d elastic scattering is currently under investigation.[20] We also mention that the observables determined in our experiment are linearly independent.[21] HRS experiment 685 at LAMPF, when it is completed ($\hat{\mathbf{S}}$-type target measurements), will provide six more observables.

In another measurement, in progress, at the Saturne II facility at Saclay, we will obtain yet another set of spin observables utilizing a 1600-MeV deuteron beam with

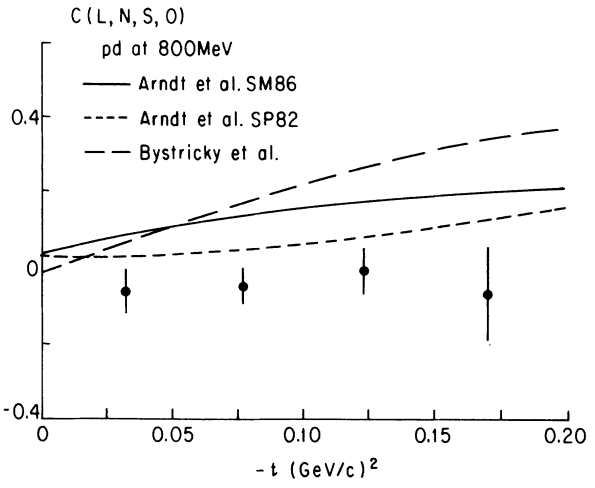

FIG. 8. The third-order spin observable, $C(L,N,S,0)$. See the caption of Fig. 3 for an explanation of the curves shown in this figure.

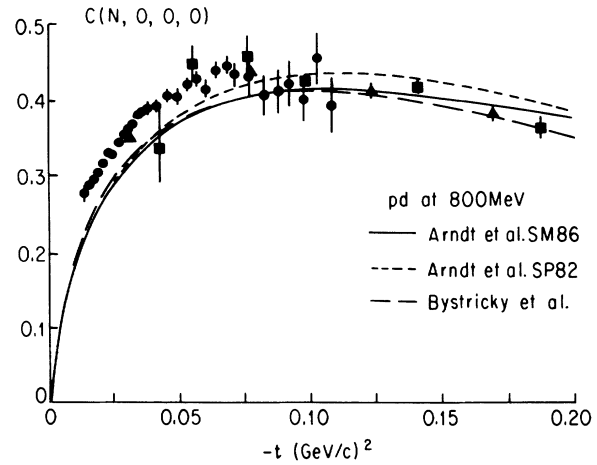

FIG. 10. The proton vector asymmetry, $C(N,0,0,0)$. See the caption of Fig. 3 for an explanation of the curves shown in this figure. The dots represent the data of Ref. 18. The triangles correspond to the data of Ref. 12, and the data points marked with squares are from Ref. 15.

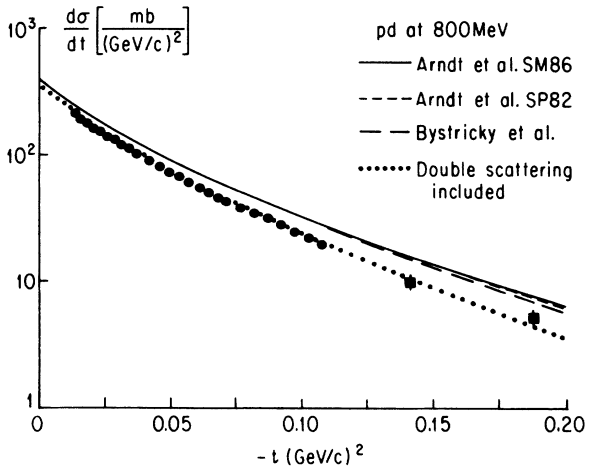

FIG. 11. The unpolarized differential cross section. See the last section of this paper for an explanation of the solid, long-dashed, and short-dashed curves shown in this figure. The dotted curve represents calculation based on the solution SP82 with the double scattering term included according to the prescription of Ref. 13. The data represented with dots are taken from Ref. 18 and the data marked with squares are from Ref. 15.

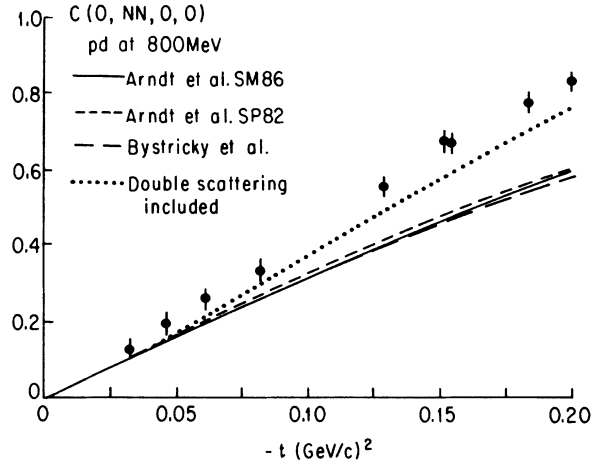

FIG. 13. The tensor asymmetry, $C(0,NN,0,0)$. See the last section of this paper for an explanation of the solid, long-dashed, and short-dashed curves shown in this figure. The dotted curve represents calculation based on the solution SP82 with the double scattering term included according to the prescription of Ref. 13. The data are taken from Ref. 6.

large tensor polarization and a polarized proton target. This will provide data at the same center-of-mass energy (i.e., equivalent to 800 MeV proton bombarding energy) for four-momentum transfers $0.2 < |t| \leq 0.7$ $(GeV/c)^2$ *larger* than those of the present experiment. These results, when combined with the measurements discussed above in this section, will be used to determine the scattering amplitude.

Another measurement (Experiment 818) scheduled for running in 1987 at LAMPF and alluded to above, in conjunction with the measurements summarized above, will provide a set of redundant observables in the larger four-momentum transfer range $[0.2 < |t| < 0.7$ $(GeV/c)^2]$. Thus, in the course of time, we may expect that the 12 complex components of the scattering amplitude in the four-momentum transfer range where single and double scattering are predominant $[|t| \leq 0.7$ $(GeV/c)^2]$ will be

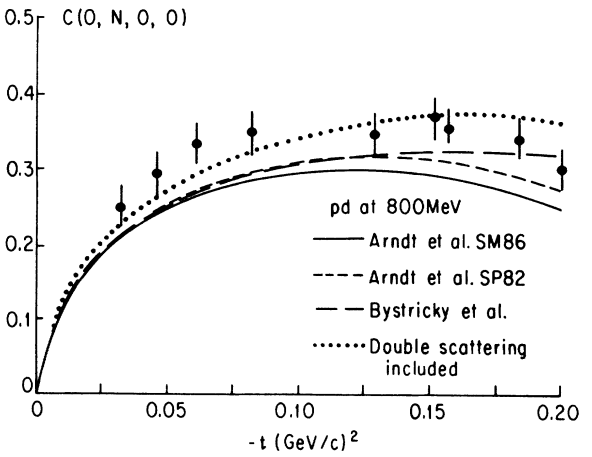

FIG. 12. The deuteron vector asymmetry, $C(0,N,0,0)$. See the last section of this paper for an explanation of the solid, long-dashed, and short-dashed curves shown in this figure. The dotted curve represents calculation based on the solution SP82 with the double scattering term included according to the prescription of Ref. 13. The data are taken from Ref. 6.

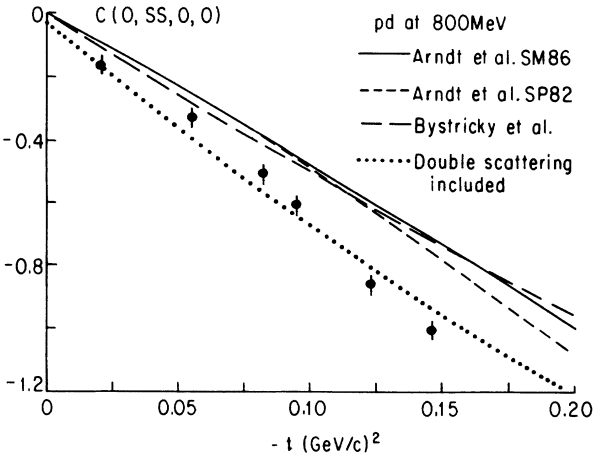

FIG. 14. The tensor asymmetry $C(0,SS,0,0)$. See the last section of this paper for an explanation of the solid, long-dashed, and short-dashed curves shown in this figure. The dotted curve represents calculation based on the solution SP82 with the double scattering term included according to the prescription of Ref. 13. The data are taken from Ref. 6.

determined experimentally with both discrete and continuous ambiguities removed, with reasonably small uncertainties. The overdetermination of the scattering amplitude, which arises because of the redundancy in the number of observables [projected to be 32 in the range $0.015 \leq |t| \leq 0.2$ $(\mathrm{GeV}/c)^2$ and 35 in the range $0.2 \leq |t| \leq 0.7$ $(\mathrm{GeV}/c)^2$] will actually provide the proton-deuterium scattering amplitude, with discrete and continuous ambiguities removed, of course, within the accuracy provided by the experimental uncertainties in the data.

ACKNOWLEDGMENTS

We wish to acknowledge the assistance of M. Krumpolc, who prepared the chrome complex used in the fully deuterated propanediol target material. We also thank the members of the HRS Program Advisory Committee and particularly the Chairman, S. Wallace, for an initial recommendation to make these measurements followed by their continued encouragement and support during the experiment and data analysis. We also wish to acknowledge the excellent support of this experiment by the LAMPF staff. We are particularly indebted to L. Agnew, MP Associate Division Leader, who carefully monitored the experiment in its planning and equipment construction phases and made the hard decisions which related to LAMPF funding and personnel support, which made it possible to implement this experiment in a timely fashion. Finally, we wish to acknowledge the loan of the ^{3}He-^{4}He refrigerator and cryostat provided by the National Laboratory for High Energy Physics (KEK). This work was supported in part by the Department of Energy.

---

*Present address: Department of Physics, Kyoto University, Kyoto 606, Japan.

†Present address: Rogalandsforskening, Postboks 2503 Ullandhang, N-4001 Stavanger, Norway.

‡Present address: Rice University, Houston, TX 77251.

§Present address: Argonne National Laboratory, Physics Division, 9700 S. Cass Avenue, Argonne, IL 60439.

**Present address: University of Texas at Austin, Austin, TX 78712, and University of Udine, Udine, Italy.

††Present address: Indiana University Cyclotron Facility, 2401 Milo B. Sampson Lane, Bloomington, IN 47405.

‡‡Present address: AT&T Asia/Pacific, Inc., 9/F., Hong Kong Club Building, 3A Chater Road, Central, Hong Kong.

[1]R. A. Arndt, L. D. Roper, R. A. Bryan, R. B. Clark, B. J. VerWest, and P. Signell, Phys. Rev. D **28**, 97 (1983); R. A. Arndt, private communication.

[2]J. Bystricky, C. Lechanoine-Leluc, and F. Lehar, Saclay Report No. DPhPE 86-13, 1986.

[3]E. Bleszynski, M. Bleszynski, and T. Jaroszewicz, in *Intersection Between Particle and Nuclear Physics (May 26–31, 1986, Lake Louise, Canada)*, Proceedings of the Second Particle and Nuclear Physics, AIP Conf. Proc. No. 150, edited by D. F. Geesaman (AIP, New York, 1986).

[4]S. Ishimoto *et al.*, Nucl. Instrum. Methods **171**, 269 (1980).

[5]M. Bleszynski, J. B. Carroll, M. Haji-Saeid, G. Igo, A. T. M. Wang, A. Sagle, C. L. Morris, R. Klem, T. Joyce, Y. Makdisi, M. Marshak, B. Mossberg, E. A. Peterson, and K. Ruddick, Phys. Lett. **106B**, 42 (1981).

[6]M. Haji-Saeid, M. Bleszynski, J. B. Carroll, G. Igo, T. Jaroszewicz, A. T. M. Wang, A. Sagle, C. L. Morris, R. Klem, T. Joyce, Y. Makdisi, M. Marshak, B. Mossberg, E. A. Peterson, and K. Ruddick, Phys. Rev. C **36**, 2010 (1987).

[7]F. Sperisen, Nucl. Instrum. Methods A **260**, 455 (1987).

[8]G. G. Ohlsen, Rep. Prog. Phys. **35**, 717 (1972).

[9]J. Kelly, private communication.

[10]J. Arvieux, S. D. Baker, R. Beurtey, M. Boivin, J. M. Cameron, T. Hasegawa, D. Hutcheon, J. Banaigs, J. Berger, A. Codino, J. Duflo, L. Goldzahl, F. Plouin, A. Boudard, G. Gaillard, Nguyen Van Sen, and C. F. Perdrisat, Nucl. Phys. **A431**, 613 (1984).

[11]G. Igo *et al.* (unpublished).

[12]D. Adams, B. Aas, E. Bleszynski, M. Bleszynski, G. Igo, C. Newsom, Y. Ohashi, G. Pauletta, F. Sperisen, C. A. Whitten, Jr., H. Fujisawa, M. Gazzaly, S. J. Greene, K. Jones, J. B. McClelland, N. Tanaka, H. Hasai, K. Iwatani, S. Ishimoto, S. Isagawa, A. Masaike, A. Okihana, and S. Okumi, Nucl. Phys. **A480**, 530 (1988).

[13]G. Alberi, M. Bleszynski, and T. Jaroszewicz, Ann. Phys. (NY) **142**, 299 (1982).

[14]L. Wolfenstein, Annu. Rev. Nucl. Sci. **6**, 43 (1956).

[15]E. Winkelman, P. R. Bevington, M. W. McNaughton, H. B. Willard, F. H. Cverna, E. P. Chamberlin, and N. S. P. King, Phys. Rev. C **21**, 2535 (1980).

[16]Sun Tsu-hsun, B. E. Bonner, M. W. McNaughton, H. Ohnuma, O. B. Van Dyck, G. S. Weston, B. Aas, E. Bleszynski, M. Bleszynski, G. J. Igo, D. J. Cremans, C. L. Hollas, K. H. McNaughton, P. J. Riley, R. F. Rodebaugh, Shen-Wu Xu, and S. E. Turpin, Phys. Rev. C **31**, 515 (1985).

[17]A. Rahbar, B. Aas, E. Bleszynski, M. Bleszynski, K. Ganezer, G. J. Igo, F. Irom, B. E. Bonner, O. Van Dyck, M. W. McNaughton, J. B. Roberts, C. Hollas, R. D. Ransome, and P. J. Riley, Phys. Lett. B **194**, 338 (1987).

[18]F. Irom, G. J. Igo, J. B. McClelland, C. A. Whitten, Jr., and M. Bleszynski, Phys. Rev. C **28**, 2380 (1983).

[19]See, for example, K. Nam, M. J. Moravscik, and G. R. Goldstein, Phys. Rev. Lett. **52**, 2305 (1984).

[20]E. Bleszynski, M. Bleszynski, and T. Jaroszewicz (unpublished).

[21]F. Sperisen, Suppl. J. Phys. Soc. Jpn. **55**, 852 (1986).